3D IMAGE RECONSTRUCTION FROM MULTI-FOCUS MICROSCOPE: AXIAL SUPER-RESOLUTION AND MULTIPLE-FRAME PROCESSING

Seunghwan Yoo[1]*, Pablo Ruiz*[1]*, Xiang Huang*[2]*, Kuan He*[1]*, Nicola J. Ferrier*[2]*, Mark Hereld*[2]*, Alan Selewa*[3]*, Matthew Daddysman*[3]*, Norbert Scherer*[3]*, Oliver Cossairt*[1]*, Aggelos K. Katsaggelos*[1]
[1]Dept. of Electrical Eng. and Computer Science, Northwestern University, Evanston, IL 60208, USA
[2]Mathematics and Computer Science Division, Argonne National Laboratory, Lemont, IL 60439, USA
[3]Dept. of Chemistry, University of Chicago, Chicago, IL 60637, USA

ABSTRACT

Multi-focus microscope (MFM) provides a way to obtain 3D information by simultaneously capturing multiple focal planes. The naive method for MFM reconstruction is to stack the sub-images with alignment. However, the resolution in the z-axis in this method is limited by the number of acquired focal planes. In this work we build on a recent reconstruction algorithm for MFM, using information from multiple frames to improve the reconstruction quality. We propose two multiple-frame MFM image reconstruction algorithms: batch and recursive approaches. In the batch approach, we take multiple MFM frames and jointly estimate the 3D image and the motion for each frame. In the recursive approach, we utilize the reconstructed image from the previous frame. Experimental results show that the proposed algorithms produce a sequence of 3D object reconstruction with high quality that enable reconstruction of dynamic extended objects.

***Index Terms*—** Multi-focus microscopy, 3D image reconstruction, total variation, multi-frame image reconstruction

1. INTRODUCTION

The conventional way to acquire a 3D image of the sample (i.e., the object) with a microscope is via sequential refocusing. Once a focal stack of the object is captured, and given the point spread function (PSF) of the optical system, a 3D deconvolution is performed to reconstruct the 3D object. However, sequential refocusing has serious disadvantages. It is too slow to accurately capture the dynamics and the stage movement for refocusing can cause perturbation of the sample. To overcome these limitations, Abrahamsson *et al.* developed the multi-focus microscopy (MFM) to capture multiple focal planes as a single snapshot [1]. MFM uses a diffractive grating or diffractive optical element (DOE) to split the light from different focal planes into separate paths and forms an array of images on the camera.

Given a single MFM measurement, a 3D volume can be generated simply by stacking the sub-images with the alignment [1]. However, in this way, one can only reconstruct as many focal planes as the number of sub-images, and the z spacing between the slices is limited to the focal shift between two adjacent sub-images. Also, it will suffer from the out-of-focus blur. Huang *et al.* proposed a reconstruction method that uses a densely z-sampled 3D PSF comprised of these 2D depth-encoded MFM images [2]. This approach handles the out-of-focus blur and results in improved resolution in the z-axis for single frame MFM images.

Because MFM is able to capture video of dynamic scenes, we can make use of multiple frames to obtain a higher quality reconstruction. The same idea has been widely used in the super-resolution (SR) literature, where the motion between different frames is taken into account to complete sub-pixel information [3–10]. Tsai and Huang first proposed to use multiple images to obtain a high resolution (HR) image but only considered translational motion [3]. Farsiu *et al.* proposed a robust estimation method by using l_1 minimization and extended the motion model to the affine transformation [4]. He *et al.* modeled the degradation with a nonlinear function to represent motion with both rotation and translation [5]. Belekos *et al.* used the maximum a posteriori (MAP) framework for video SR [6] and Babacan *et al.* proposed a variational Bayesian framework for multiple-frame SR [7]. Liu *et al.* proposed a MAP based video SR method that jointly estimates the HR image, blur, motion, and noise. They used an optical flow algorithm to estimate local motion [8]. Recent learning-based video SR methods also utilized an optical flow algorithm for motion estimation [9, 10].

All the methods described above were developed for 2D image SR. Here we extend multiple-frame (MF) image SR schemes to 3D space to obtain a higher resolution along the z-axis in MFM. We build on single frame MFM reconstruction approach in [2] and improve the reconstruction using multiple frames. We propose two approaches for MF reconstruction: the batch approach which exploits the multiple neighboring frames, and the recursive approach which uses the 3D reconstruction obtained for the previous frames. The proposed methods can also be applied to a broader range of inverse problems with multiple observations, such as, 3D image reconstruction from conventional microscopy or uncalibrated tomography [11].

The paper is organized as follows. Single frame reconstruction from [2] is summarized in Section 2 using notation consistent with the rest of the paper. The MF reconstructions algorithms are introduced in Section 3. Experimental results and discussion are provided in Section 4 and we conclude our paper in Section 5.

2. SINGLE-FRAME MFM RECONSTRUCTION

2.1. Acquisition Model

Fig. 1 (a) illustrates our MFM system. The DOE splits the light from different focal planes, forming $K \times K$ tiles as shown in Fig. 1 (b). Each tile corresponds with the image obtained for a different focal plane. Because it is a linear spatially invariant system, its whole optical system can be characterized by its PSF. The 3D PSF is estimated by sequential refocusing with a fixed fluorescent bead.

This work was supported as part of the Small Worlds project by funding through the Biological Systems Science Division, Office of Biological and Environmental Research, Office of Science, U.S. Dept. of Energy, under Contract DE-AC02-06CH11357.

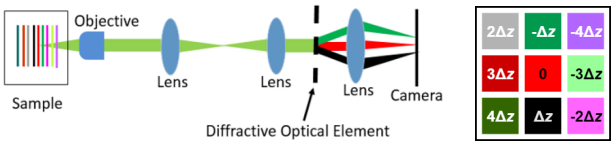

(a) (b)

Fig. 1: Schematics and captured image of MFM.

Let $f \in \mathbb{R}^{N_x \times N_y \times N_z}$, $g \in \mathbb{R}^{M_x \times M_y}$, and $h \in \mathbb{R}^{M_x \times M_y \times M_z}$ denote a 3D object, its MFM measurement, and the 3D PSF of the MFM, respectively. The acquisition process of MFM can be modeled as the extraction of one plane (suppose $z = 0$) after 3D convolution of f and h, and equivalently as the sum of 2D convolutions of $f(x, y; -z)$ and $h(x, y; z)$, plus additive Gaussian noise $\epsilon \in \mathbb{R}^{M_x \times M_y}$ as

$$\begin{aligned} g(x,y) &= h(x,y,z) *_{3D} f(x,y,z)\big|_{z=0} + \epsilon(x,y) \\ &= \sum_{z=-\lfloor N_z/2 \rfloor}^{\lfloor N_z/2 \rfloor} h(x,y;z) *_{2D} f(x,y;-z) + \epsilon(x,y), \end{aligned} \tag{1}$$

where $*_{3D}$ and $*_{2D}$ denote the 3D convolution and the 2D convolution operators, respectively. Eq. 1 can also be expressed in matrix-vector notation as

$$\mathbf{g} = \mathbf{H}\mathbf{f} + \boldsymbol{\epsilon} \tag{2}$$

where $\mathbf{f} \in \mathbb{R}^{N_x N_y N_z \times 1}$, $\mathbf{g} \in \mathbb{R}^{M_x M_y \times 1}$, and $\boldsymbol{\epsilon} \in R^{M_x M_y \times 1}$ are vectorized f, g, and ϵ, respectively, and $\mathbf{H} \in \mathbb{R}^{M_x M_y \times N_x N_y N_z}$ denotes the MFM PSF matrix.

2.2. Single-Frame Reconstruction (SFR)

To reconstruct a 3D object, $\mathbf{f}$, when provided a MFM image, $\mathbf{g}$, and the MFM PSF matrix, $\mathbf{H}$, we can formulate the inverse problem as in [2]. Assuming Gaussian noise, a regularized least squares method to reconstruct $\mathbf{f}$ is formulated as follows:

$$\hat{\mathbf{f}} = \arg\min_{\mathbf{f}} \ \|\mathbf{g} - \mathbf{H}\mathbf{f}\|_2^2 + \lambda\Phi(\mathbf{f}), \quad \text{subject to } \mathbf{f} \geq 0 \tag{3}$$

where λ is a regularizing parameter, and $\Phi(\cdot)$ is a regularizer function. In this paper we chose the 3D total variation (TV) regularizer because it encourages piecewise smoothness of the signal by enforcing sparsity in the gradient domain. It is suitable for extended objects, such as bacteria that we want to reconstruct. The TV regularizer for a 3D object, $\mathbf{f}$, is defined as

$$\Phi(\mathbf{f}) = \sum_i \sqrt{(\Delta_i^x \mathbf{f})^2 + (\Delta_i^y \mathbf{f})^2 + (\Delta_i^z \mathbf{f})^2} \tag{4}$$

where i is a voxel index and $\Delta_i^x \mathbf{f}$, $\Delta_i^y \mathbf{f}$, and $\Delta_i^z \mathbf{f}$ denote first-order difference operators in the x, y, and z directions, respectively. Eq. 3 is solved by employing the two-step iterative shrinkage/thresholding (TwIST) algorithm [12] with the projected gradient scheme for the non-negativity constraint. Note that the choice of the regularizing parameter, λ, is important for the quality of reconstruction. If it is too large or too small, it converges to a poor solution. In our experiments, we performed an exhaustive search for this parameter to obtain an optimal reconstruction.

3. MULTIPLE-FRAME MFM RECONSTRUCTION

Given a sequence of MFM images, we can use multiple MFM images to achieve a higher quality 3D reconstruction. We first describe two acquisition models for MF MFM images and introduce two approaches for the MF MFM reconstruction. Here we assume that there is a single rigid object in the sample space and model the motion as a rigid transformation that only includes 3D translation and 3D rotation.

3.1. Acquisition Model

The first model for the acquisition process describes a mapping from a 3D object at k-th frame, $\mathbf{f}_k \in R^{N_x N_y N_z \times 1}$, to the captured MFM image, $\mathbf{g}_k \in R^{M_x M_y \times 1}$. Let $\mathbf{H} \in R^{M_x M_y \times N_x N_y N_z}$ and $\boldsymbol{\epsilon}_k \in R^{M_x M_y \times 1}$ denote the MFM PSF matrix and the noise in k-th frame respectively. Then, the acquisition process is modeled as

$$\mathbf{g}_k = \mathbf{H}\mathbf{f}_k + \boldsymbol{\epsilon}_k. \tag{5}$$

which is the same form as Eq. 2 in Section 2 for the SFR algorithm. The acquisition model in Eq. 5 can be extended by considering the relationship between frames as

$$\mathbf{g}_k = \mathbf{H}\mathbf{M}_{l,k}(\boldsymbol{\alpha}_{l,k})\mathbf{f}_l + \boldsymbol{\epsilon}_{l,k} \tag{6}$$

where $\boldsymbol{\alpha}_{l,k}$ and $\mathbf{M}_{l,k}(\boldsymbol{\alpha}_{l,k})$ denote the motion parameters for the 3D object from l-th frame to k-th frame and the warping matrix corresponding to $\boldsymbol{\alpha}_{l,k}$, and $\boldsymbol{\epsilon}_{l,k}$ is a Gaussian noise term. $\boldsymbol{\alpha}_{l,k}$ consists of three parameters for 3D translation and three parameters for 3D rotation since rigid transformation is assumed for the motion. Note that, in this model, every MFM measurement originates from the reference object, $\mathbf{f}_l$, through a geometric transformation and MFM imaging with noise.

3.2. Batch Approach

Based on the acquisition model in Eq. 6, we suggest to use a batch of MFM measurements to reconstruct one frame, $\mathbf{f}_l$, and we call it the batch approach for MF reconstruction. We formulate the optimization problem to estimate $\mathbf{f}_l$ for the batch approach as

$$\begin{aligned} \{\hat{\mathbf{f}}_l, \hat{\boldsymbol{\alpha}}_{l,k}\} = \arg\min_{\mathbf{f}_l \geq 0, \boldsymbol{\alpha}_{l,k}} & \sum_{k=l-m}^{l+m} \|\mathbf{g}_k - \mathbf{H}\mathbf{M}_{l,k}(\boldsymbol{\alpha}_{l,k})\mathbf{f}_l\|_2^2 \\ & + \lambda\Phi(\mathbf{f}_l) + \omega \sum_{k=l-m}^{l+m} \|\boldsymbol{\alpha}_{l,k}\|_2^2 \end{aligned} \tag{7}$$

where m is a positive number that determines the number of neighboring frames used in the reconstruction, and ω is the regularizing parameter for $\boldsymbol{\alpha}_{l,k}$.

The first term in Eq. 7 is the data fidelity term based on the acquisition model in Eq. 6. In principle, the whole sequence of MFM image can be used for the reconstruction of $\mathbf{f}_l$, but it is computationally demanding and frames far in time can possibly degrade the reconstruction quality due to large mis-registration error. Therefore, we use a batch of frames around $\mathbf{f}_l$. The last term in Eq. 7 is a regularizer for the motion parameters. Since the motion between two frames is small for a short period of time, we chose the l_2 norm to enforce small values for $\boldsymbol{\alpha}_{l,k}$. ω is chosen empirically and is set to small values.

The alternating descent scheme is applied to solve the multivariable non-convex problem of Eq. 7. We solve for $\mathbf{f}_l$ while fixing $\boldsymbol{\alpha}_{l,k}$ first, and then solve for the motion parameters set by set while fixing $\mathbf{f}_l$ and the other motion parameter sets. Note that in this approach we have $2m$ sets of motion parameters to estimate ($\boldsymbol{\alpha}_{l,k}$ for $k = l-m, \cdots, -1, 1, \cdots, l+m$). The alternation is repeated until it converges.

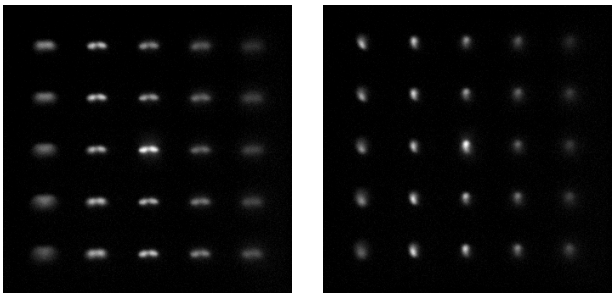

(a) (b)

Fig. 2: Simulated MFM images with a bacterium-like object with Gaussian noise ($\sigma_n = 0.02$). (a) The object lies in the xy plane at frame 3, and (b) stands along the z-axis at frame 21.

3.3. Recursive Approach

Based on Eq. 5, each frame can be reconstructed by the SFR method as described in Section 2. For $k = 1, \cdots, S$, it can be expressed as

$$\hat{\mathbf{f}}_k = \arg\min_{\mathbf{f_k} \geq 0} \|\mathbf{g}_k - \mathbf{H}\mathbf{f}_k\|_2^2 + \lambda\Phi(\mathbf{f}_k). \tag{8}$$

Here we can exploit the information from previous frames in a recursive manner by using the 3D reconstruction data from the previous frame. Since we assume the 3D object is rigid, we add a constraint that the reconstruction at k-th frame should be the same as the reconstruction at $(k-1)$-th frame under a rigid transformation as

$$\begin{aligned}\{\hat{\mathbf{f}}_k, \hat{\boldsymbol{\alpha}}_{k-1,k}\} = \arg\min_{\mathbf{f}_k \geq 0, \boldsymbol{\alpha}_{k-1,k}} & \|\mathbf{g}_k - \mathbf{H}\mathbf{f}_k\|_2^2 + \lambda\Phi(\mathbf{f}_k) \\ & + \eta\|\mathbf{f}_k - \mathbf{M}_{k-1,k}(\boldsymbol{\alpha}_{k-1,k})\mathbf{f}_{k-1}\|_2^2,\end{aligned} \tag{9}$$

where λ and η are the regularizing parameters for each regularizer term, which can be chosen by exhaustive search.

Eq. 9 is a non-convex optimization problem with two unknown variables, $\mathbf{f}_k$ and $\boldsymbol{\alpha}_{k-1,k}$. Similarly to the batch approach, we use the alternating descent algorithm to solve for each variable in an alternating fashion until convergence.

4. EXPERIMENTAL RESULTS

In this section, we evaluate the performance of single-frame reconstruction (SFR), multiple-frame batch approach (MF batch) and multiple-frame recursive approach (MF recursive), on both synthetic and real datasets.

4.1. Synthetic Experiment

For the synthetic experiment, a 3D image of a double-lobe bacterium was acquired by using confocal microscopy. The 3D image is scaled, cropped, and located in the center of the space of $50 \times 50 \times 51$. 30 frames were generated by sequentially adding to each new frame a rotation of 5° along the y-axis and 2° along the z-axis, and a 3D random shift generated by multivariate Gaussian with mean 0 and covariance matrix $I_{3\times3}$. Fig. 3 (a) and Fig. 4 (a) show the simulated 3D object at different frames. To visualize the 3D image more effectively, we used a colormap such that blue and red colors indicate the lowest and the highest intensity respectively, and display three projections onto the xy, yz, and zx planes as well. The object lies along xy plane at frame 3, and stands along the z direction at frame 21. The obtained frames are used as ground truth in our experiments.

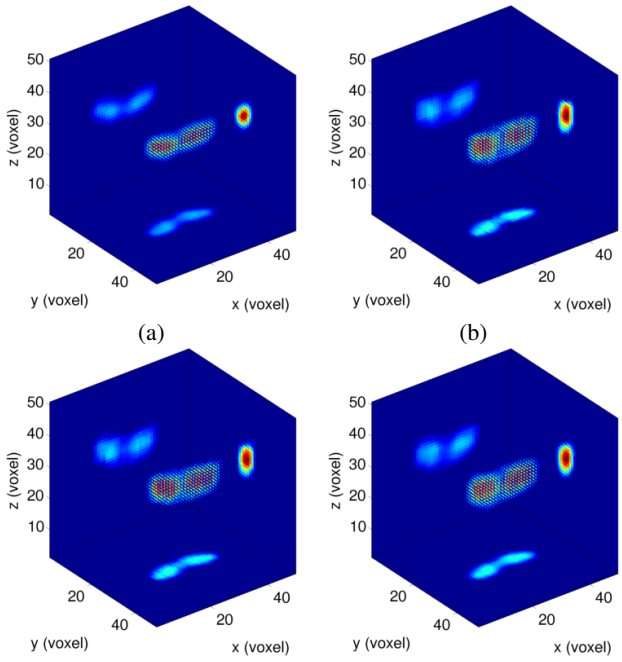

Fig. 3: Reconstructed 3D images at frame 3 with σ_n = 0.02. (a) Ground truth, (b) SFR, PSNR:37.24, SSIM:0.9868, (c) MF batch ($m = 2$), PSNR:38.13, SSIM:0.9887, (d) MF recursive, PSNR:37.79, SSIM:0.9877.

To simulate the MFM acquisition model, each frame is degraded according to Eq. 1, with a scaled version of the measured PSF. We generated observations for two different standard deviation values of the Gaussian noise $\sigma_n = 0.01$ and $\sigma_n = 0.02$. Fig. 2 shows the simulated MFM images at different frames with $\sigma_n = 0.02$.

Figures 3 and 4 show the original and the reconstructed 3D images, with noise $\sigma_n = 0.02$, at frames 3 and 21 out of 30 frames. For both frames, we observe that the reconstructions become elongated along the z axis, which is caused by the missing cone problem in microscopy imaging [13, 14]. Nevertheless, we can observe the reconstructions are very similar to the ground truth, especially along the xy plane. The quality between reconstruction methods is distinguished at frame 21 where SFR fails reconstructing the double lobe. However, MF reconstruction approaches reconstruct the two lobes as can be clearly seen in the projections. The reconstruction of MF batch is better than SFR but it is visually noisier than MF recursive.

Table 1 summarizes the overall performance of the MFM reconstruction algorithms in average peak signal-to-noise ratio (PSNR) and structural similarity index (SSIM). The MF reconstruction methods improve the performance, and MF recursive results in the most significant improvement in average. These numbers match the visual quality from Figs. 3 and 4. As the more neighboring frames are used, MF batch results in better performance but with more intense computation.

The plots in Fig. 5 show the PSNR values for all the frames. They tell a few things about the reconstruction methods. First, the MF approaches give better reconstruction compared to the SFR method. The PSNRs of the MF approaches are higher than those of the SFR method at most of the frames. Second, MF batch follows the trend of the SFR, but produces higher quality reconstruction than SFR by using multiple observation. The more observation,

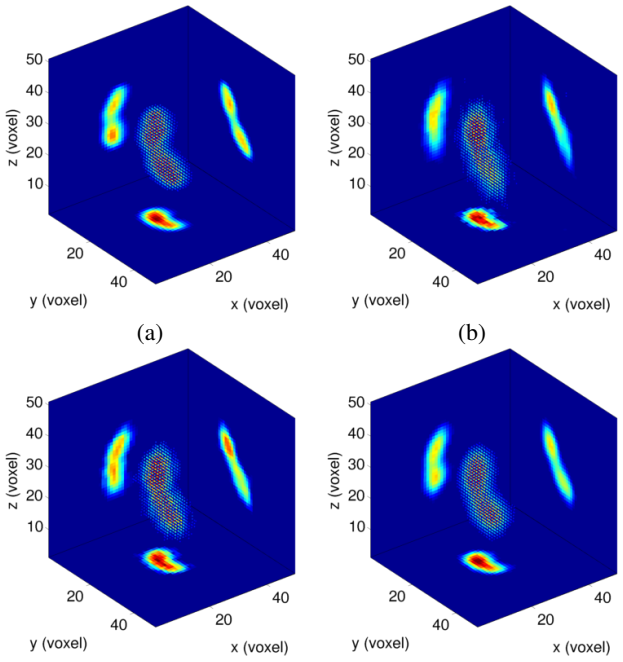

Fig. 4: Reconstructed 3D images at frame 21 with σ_n = 0.02. (a) Ground truth, (b) SFR, PSNR:36.39, SSIM:0.9747, (c) MF batch ($m = 2$), PSNR:38.80, SSIM:0.9835, and (d) MF recursive, PSNR:40.97, SSIM:0.9866.

the better reconstruction. Third, the performance of MF recursive depends on the previous reconstruction. The reconstruction quality does not change as abruptly as the other methods frame by frame. Because it encourages the reconstruction to be the same as previous reconstruction, it tries to keep the 3D shape. In this way, it produces more consistent 3D reconstruction over the sequence.

Table 1 also shows the average running time of the reconstruction in the unit of minute. The MF reconstruction algorithms takes more time since they have more data to process and have to estimate the motion between frames in addition to the 3D image in an iterative manner. The batch approach uses $(2m + 1)$ times as much data as SFR and also it has $2m$ sets of the motion parameters to estimate. For the recursive approach, it adds as much data as the reconstruction object for image estimation, and has one set of motion parameters to estimate. Note that the time in the table for SFR does not include the time for the exhaustive search for an optimal λ.

4.2. Real Experiment

A tumbling bacterium was captured with our MFM system [2]. The frame rate was about 30 fps and the illumination time was 20 ms per frame. The effective pixel size is $98nm \times 98nm$ and the pixel

Table 1: Performance and running time of MFM image reconstruction algorithms. Average PSNR, SSIM, and running time are calculated over 26 frames. Running time is recorded in the unit of minute.

	$\sigma_n = 0.01$			$\sigma_n = 0.02$		
Methods	PSNR	SSIM	Time	PSNR	SSIM	Time
SFR	38.30	0.9868	1.12	36.47	0.9786	0.83
MF batch, $m = 1$	39.04	0.9899	19.97	37.31	0.9786	36.03
MF batch, $m = 2$	40.05	0.9919	49.58	38.17	0.9814	123.30
MF recursive	40.20	0.9897	4.36	39.57	0.9842	4.37

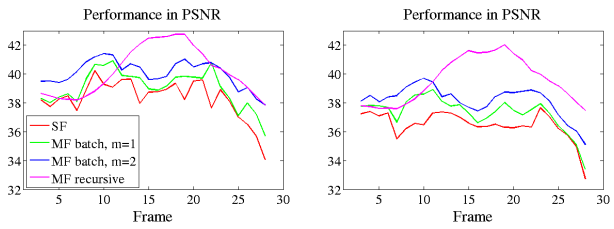

Fig. 5: PSNRs for each frame, (a) $\sigma_n = 0.01$, (b) $\sigma_n = 0.02$.

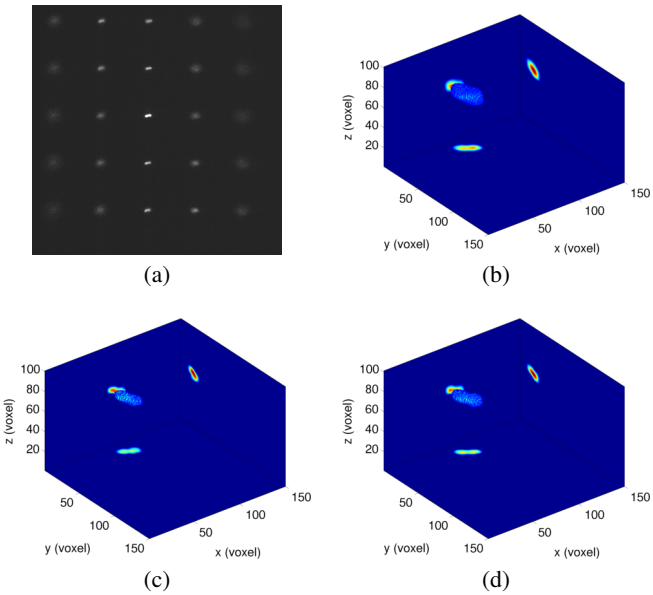

Fig. 6: Reconstructed 3D images from the real data at frame 22 (a) MFM measurement, (b) SFR, (c) MF batch approach, and (d) MF recursive approach.

resolution of the camera is 1024×1024. Fig. 6 (a) shows an MFM image at frame 22.

For real data, the reconstruction results are evaluated by visual quality. Fig. 6 shows the MFM measurement and the reconstruction results with the three algorithms: SFR, MF batch, and MF recursive at frame 22. While all three methods reconstruct the 3D image of the bacterium that conforms to the size and the shape of the bacteria that we already know, the MF reconstruction methods produce sharper 3D images than SFR. Also, SFR becomes more sensitive to the choice of λ for the real data so we tried up to 15 values of λ to obtain reasonable reconstruction quality.

5. CONCLUSION

We have developed two multiple-frame (MF) 3D image reconstruction algorithms for MFM: MF batch, and MF recursive. Our methods outperform the single-frame reconstruction, achieving higher quality image reconstruction in axial super-resolution. MF batch uses a batch of neighboring MFM images for reconstruction while MF recursive utilizes the reconstructed 3D image from the previous frame. Experimental results with both synthetic and real data show the effectiveness of our methods.

6. REFERENCES

[1] S. Abrahamsson, J. Chen, B. Hajj, S. Stallinga, A. Y. Katsov, J. Wisniewski, G. Mizuguchi, P. Soule, F. Mueller, C. D. Darzacq, X. Darzacq, C. Wu, C. I. Bargmann, D. A Agard, M. Dahan, and M. G. L. Gustafsson, "Fast multicolor 3D imaging using aberration-corrected multifocus microscopy," *Nature Methods*, vol. 10, no. 1, pp. 60–63, 2012.

[2] X. Huang, A. Selewa, X. Wang, M. K. Daddysman, I. Gdor, R. Wilton, K. M. Kemner, S. Yoo, A. K. Katsaggelos, O. Cossairt, N. J. Ferrier, M. Hereld, and N. F. Scherer, "3D snapshot microscopy of extended objects," arXiv:1802.01565, 2018.

[3] R. Y. Tsai and T.S. Huang, "Multiframe image restoration and registration," *Adv. Comput. Vis. Image Process.*, vol. 1, no. 2, pp. 317–339, 1984.

[4] S. Farsiu, D. Robinson, M. Elad, and P. Milanfar, "Fast and Robust Multi-Frame Super-Resolution," *IEEE Transactions on Image Processing*, vol. 13, no. 10, pp. 1327–1344, 2004.

[5] Y. He, K. H. Yap, L. Chen, and L. P. Chau, "A nonlinear least square technique for simultaneous image registration and super-resolution," *IEEE Transactions on Image Processing*, vol. 16, no. 11, pp. 2830–2841, 2007.

[6] S. P. Belekos, N. P. Galatsanos, and A. K. Katsaggelos, "Maximum a posteriori video super-resolution using a new multichannel image prior," *IEEE Transactions on Image Processing*, vol. 19, no. 6, pp. 1451–1464, 2010.

[7] S. D. Babacan, R. Molina, and A. K. Katsaggelos, "Variational Bayesian Super Resolution.," *IEEE Transactions on Image Processing*, vol. 20, no. 4, pp. 984–999, 2011.

[8] C. Liu and D. Sun, "On Bayesian Adaptive Video Super Resolution," *IEEE Transactions on Pattern Analysis and Machine Intelligence*, vol. 36(2), no. 2, pp. 346–360, 2014.

[9] A. Kappeler, S. Yoo, Q. Dai, and A. K. Katsaggelos, "Video Super-Resolution with Convolutional Neural Networks," *IEEE Transactions on Computational Imaging*, vol. PP, no. 99, pp. 1–1, 2016.

[10] Q. Dai, S. Yoo, A. Kappeler, and A. K. Katsaggelos, "Sparse Representation-Based Multiple Frame Video Super-Resolution," *IEEE Transactions on Image Processing*, vol. 26, no. 2, pp. 765–781, 2017.

[11] D. Grsoy, Y. P. Hong, K. He, K. Hujsak, S. Yoo, S. Chen, Y. Li, M. Ge, L. M. Miller, Y. S. Chu, V. De Andrade, K. He, O. Cossairt, A. K. Katsaggelos, and C. Jacobsen, "Rapid alignment of nanotomography data using joint iterative reconstruction and reprojection," *Scientific Reports*, vol. 7, no. 1, 12 2017.

[12] J. M. Bioucas-Dias and M. A. T. Figueiredo, "A new TwIST: Two-step iterative shrinkage/thresholding algorithms for image restoration," *IEEE Transactions on Image Processing*, vol. 16, no. 12, pp. 2992–3004, 2007.

[13] F. Macias-Garza, A. C. Bovik, K. R. Diller, S. J. Aggarwal, and J. K. Aggarwal, "The missing cone problem and low-pass distortion in optical serial sectioning microscopy," in *International Conference on Acoustics, Speech, and Signal Processing*. 1988, pp. 890–893, IEEE.

[14] J. Lim, K. Lee, K. Jin, S. Shin, S. Lee, Y. Park, and J. Ye, "Comparative study of iterative reconstruction algorithms for missing cone problems in optical diffraction tomography.," *Optics express*, vol. 23, no. 13, pp. 16933–48, jun 2015.